Uncertainty Quantification for Transient Thermal Management

Jason D. Muff[1], Rama Subba Reddy Gorla[1,*] and Edwin Forster[2]

[1]*Department of Aeronautics and Astronautics, 2950 Hobson Way, WPAFB, OH, 45433, USA*

[2]*Design and Analysis Branch, Aerospace Systems Directorate, Air Force Research Laboratory (AFRL/RQVC), 2210 Eighth St., WPAFB, OH, 45433-7542, USA*

Abstract: Thermal resource management (TRM) of onboard hypersonic vehicles is an important field of research and development, and considerable attention has been received from the scientific community in the past few decades. A scramjet engine at hypersonic speed warrants stringent cooling requirements to manage its thermal load. Therefore, managing thermal loads in an advanced engine to power future aircraft is challenging. The US Air Force Research Laboratory (AFRL) is investigating ways in which heat can be dissipated to cool hypersonic vehicles. The uncertainty quantification in a transient heat rejection system is analyzed. The stochastic nature of the initial condition and heat rejection boundary condition is introduced to define the temperature distribution in the system. Results are presented for the temperature variation as a result of uncertainties in the initial condition and Biot number at the boundary where heat is rejected. The terms that impact the overall uncertainty in the transient regions are discussed.

Keywords: Uncertainty quantification, Transient heat transfer, Thermal management, Monte Carlo method, Statistical analysis.

1. INTRODUCTION

THERE are often situations in which temperature regulation is critical to the survival of aerospace systems. In recent years, hypersonic vehicles have been a focal point in research and development around the world. One of the greatest challenges faced is the exchange of heat on a hypersonic body, especially with the extreme temperatures that are often associated with aerodynamic heating experienced in hypersonic flight [1].

In hypersonic flight, material properties of the vehicles can have significant implications on a system's survivability and may impact mission success if extreme temperatures cause degradation to the integrity of the system. Furthermore, material properties may have a degree of uncertainty in their characteristics due to manufacturing processes, imperfections in manufacturing, or imprecision of measurements for component fabrication. Uncertainty in an initial condition of a material and its thermal management characteristics can propagate through time, making it difficult to predict the transient characteristics of the system.

Due to the extreme temperatures experienced in hypersonic flight, increasingly complex thermal management systems are being developed. These systems often require the movement of fuel for cooling and the implementation of heat exchangers to maintain vehicle viability [2]. If there is uncertainty in the heat exchange at a top level, the overall system may need to be modified to ensure that no component limitation is exceeded.

Uncertainty analysis has become a more recent field of study that has been applied to many different scientific fields. Several numerical methods have been developed and applied in simple problems. Some of these methods have matured to the point where numerical integration and numerical simulations may be implemented with more complex, multi-variable problems [3]. Other techniques have also been developed and utilized to optimize trajectories for the uncertainty of flight conditions when vehicles use PID controllers [4].

Previous uncertainty research has been conducted on one-dimensional heat transfer with a constant heat flux boundary condition and was compared to a high-fidelity experimental model. This shows that there is value in this method of uncertainty modeling and offers opportunity to further quantify this setup in simulation. This specific set of research explored the implications of thermal management for components including electronics, but it could also be applied to other scenarios as well due to the non-dimensional methodology [5]. Another paper explored a mathematical model with a very similar simulation setup and commented specifically on the time evolution of the stochastic characteristics [6].

A stochastic or random process in probability is the counterpart to a deterministic process. Instead of dealing with only one possible outcome of the temporal evolution of the process, in a stochastic or random

*Address correspondence to this author at Department of Aeronautics and Astronautics, 2950 Hobson Way, WPAFB, OH, 45433, USA;
E-mail: rama.gorla@us.as.mil

E-ISSN: 3110-9780/25

process, there is some indeterminacy in temporal evolution described by probability distributions. This means that there are many possibilities the process might reach, but some paths may be more probable and others less so.

This paper explores a one-dimensional plate with a constant temperature boundary condition on one surface and a convective boundary condition on the other. This is representative of a simplified plate that may be present on a hypersonic vehicle. Material properties of this simulation are represented in the value known as the Biot number, which is the ratio of internal conduction resistance to the external convective resistance of the body. With uncertainty in the material properties, the convective heat transfer coefficient, *h*, or any of the initial temperature conditions of the system, errors are expected to propagate through the model during unsteady, transient simulations. The goal of this paper is to characterize non-dimensional temperature and non-dimensional heat flux behavior to determine the factors that have the greatest risk of exceeding known thermal management limitations.

2. MODEL DESCRIPTION AND DEVELOPMENT

The problem assessed in this paper is a one-dimensional heat transfer scenario with a constant temperature boundary condition on the top surface and a convective heat transfer boundary condition along the bottom surface. This is shown in Figure **1**. Once this model was established, the following heat balance equation was analyzed to describe the behavior of the heat transfer scenario across the plate.

$$k\frac{\partial^2 T}{\partial x^2} = \rho c_p \frac{\partial T}{\partial t} \quad (1)$$

Where *k* is the thermal conductivity of the material (*W/m·K*), ρ is the density of the material (*kg/m*^{3}), and c_p is the specific heat of the material (*J/(kg·K)*). This equation is then subject to the following boundary and initial conditions:

$$T(0,t) = T_i \quad (2)$$

$$-k\left.\frac{\partial T}{\partial x}\right|_{x=L} = h(T - T_\infty) \quad (3)$$

$$T(x,0) = A + Bx \quad (4)$$

The equations above are non-homogeneous. Therefore, a solution is assumed to have the following form with both a steady and unsteady component:

$$T(x,t) = S(x) + U(x,t) \quad (5)$$

Using the separation of variables method, the steady state solution is determined as:

$$S(x) = T_i + \frac{h}{hL + k}(T_\infty - T_i)x \quad (6)$$

And the unsteady solution is:

$$U(x,t) = \sum_{n=1}^{\infty} A_n \sin(\lambda_n x)\, e^{-\lambda_n^2 \alpha t} \quad (7)$$

$$A_n = \frac{2(A - T_i)[\lambda_n L + Bi\, sin(\lambda_n L)]}{(\lambda_n L)^2 + Bi\, sin^2(\lambda_n L)} + \frac{2[BL(Bi+1) + Bi(T_i - T_\infty)]\sin(\lambda_n L)}{(\lambda_n L)^2 + Bi\, sin^2(\lambda_n L)} \quad (8)$$

With the eigenvalues, λ_n defined by the following eigenfunction:

$$\lambda_n L cos(\lambda_n L) + Bi \sin(\lambda_n L) = 0$$

Where the Biot number, $Bi = \frac{hL}{k}$

The solution for $T(x,t)$ can then be written by combining Eq. (6) and Eq. (7) into Eq. (5) and simplifying.

$$T(x,t) = T_i + \frac{Bi}{(Bi+1)}(T_\infty - T_i)\frac{x}{L} + \sum_{n=1}^{\infty} A_n \sin(\lambda_n x)\, e^{-\lambda_n^2 \alpha t} \quad (9)$$

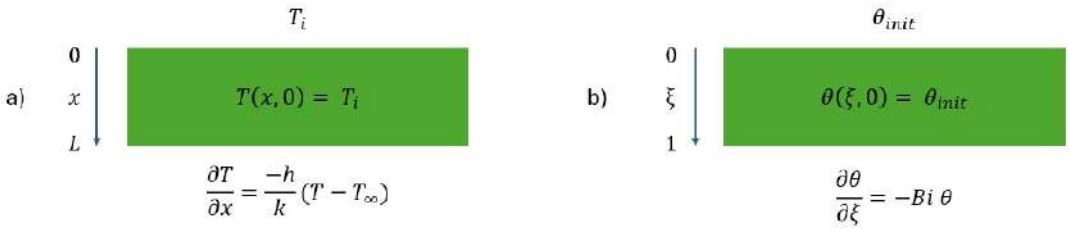

Figure 1: Description of heat transfer model: **a**) dimensional layout, initial conditions, and boundary conditions, **b**) non-dimensional layout, initial conditions, and boundary conditions.

To apply this simulation model to a variety of different materials and plate dimensions, the parameters must be non-dimensionalized. This requires the following definitions to be incorporated into the solution found in Eq. (9).

$$\theta = \frac{T - T_\infty}{T_i - T_\infty}$$

$$\xi = \frac{x}{L}$$

$$\tau = \frac{\alpha t}{L^2}$$

$$\beta_n = \lambda_n L$$

Equation (9) can then be written as follows to represent the non-dimensional temperature for a given non-dimensional coordinate and non-dimensional time.

$$\theta(\xi, \tau) = 1 - \frac{Bi}{Bi + 1}\xi + \sum A_n \sin(\beta_n \xi)\, e^{-{\beta_n}^2 \tau} \quad (10)$$

$$\theta_{init} = F_0 + F_1 \xi \quad (11)$$

$$A_n = \frac{2(F_0 - 1)(\beta_n + Bi \sin(\beta_n))}{{\beta_n}^2 + Bi\, sin^2(\beta_n)} + \frac{2[F_1(Bi + 1) + Bi] \sin(\beta_n)}{{\beta_n}^2 + Bi\, sin^2(\beta_n)} \quad (12)$$

$F_0 = \frac{A - T_\infty}{T_i - T_\infty}$ and $F_1 = \frac{BL}{T_i - T_\infty}$

Where eigenvalues, β_n, are calculated from the following eigenfunction:

$$\beta_n \cot(\beta_n) + Bi = 0 \quad (13)$$

Finally, the following equation is developed to represent the non-dimensional temperature difference across the one-dimensional plate. This is one of the two metrics that will be discussed in the results.

$$\Delta\theta = \theta(0, \tau) - \theta(1, \tau) \quad (14)$$

$$\Delta\theta = \frac{Bi}{Bi + 1} - \sum A_n \sin(\beta_n)\, e^{-{\beta_n}^2 \tau} \quad (15)$$

After development of the expression of the non-dimensional temperature difference across the plate, the non-dimensional heat flux at the top surface of the plate ($\xi = 0$) is calculated and plotted for observations. This term is important as it is the point on the plate that experiences the most extreme heat flux during any given heat exchange scenario. Non-dimensional heat flux can be represented by $\theta'(0, \tau)$. Equation (16) represents the non-dimensional heat flux. This is the second metric that will be discussed in the results section of this paper.

$$\theta'(0, \tau) = -\frac{Bi}{Bi + 1} + \sum A_n \beta_n e^{{\beta_n}^2 \tau} \quad (16)$$

3. STOCHASTIC SIMULATION METHODOLOGY

After the development of the expression of the non-dimensional temperature difference across the plate, $\Delta\theta$, and the non-dimensional heat flux at the upper surface of the plate, $\theta'(0, \tau)$, Monte-Carlo Simulations were conducted to observe the behavior of the sample when uncertainty was introduced to various parameters.

The three variables that had uncertainty introduced to them are the Biot number, Bi, the dimensionless constant describing initial temperature at the top of the plate, F_0, and the dimensionless constant parameterizing initial temperature variation across the plate, F_1. For each term, a normal distribution was randomly generated with a standard deviation scaled appropriately to have 3 standard deviations represent +/- 10% variation in the term. In the Monte-Carlo Simulation, 100 random values were sampled for Bi, F_0, and F_1. These conditions were implemented into Equations (12), (13), (15), and (16) to generate the results, which were then plotted against non-dimensional time from 0 to 1000. A computer was used to iterate calculations to find eigenvalues for each randomly selected Biot number. The initial guesses for this iterative method came from a known table of solutions to Eq. (12) [7].

A brief sample size study was conducted to verify the accuracy of the choice of 100 samples. This study was conducted specifically for the case where $Bi_\mu = 0.1$, $F_{0\mu} = 1$, and $F_{1\mu} = 0.5$. At this condition, 10, 20, and 100 samples were gathered and processed through the time dependent simulation. Afterwards, the results were averaged and compared to the no-uncertainty case. This was accomplished 50 times for each sample size test group and is shown in Figure **2**.

100 samples was determined to be a sufficiently large sample size for the simulations conducted on $\Delta\theta$. The greatest spread occurred at the initial time step, and the randomly sampled averages converged to a variation of about 0.01 from the no-uncertainty case. However, when conducting the $\theta'(0)$ simulations, the spread from the no-uncertainty case was nearly 0.05. This would likely need further refinement in future studies, however it was not accomplished due to computational limitations.

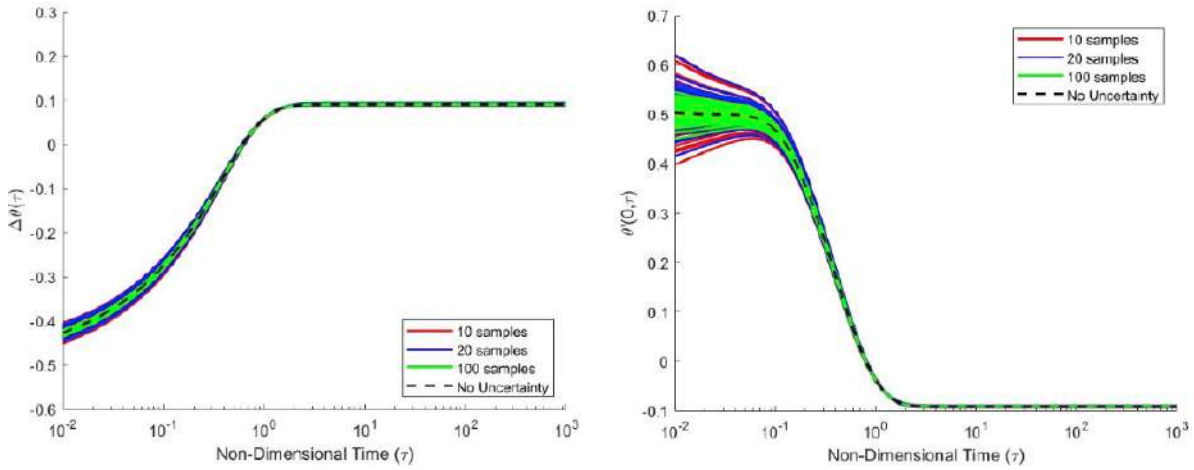

a **b**

Figure 2: Sample study for case with $\boldsymbol{Bi_{\mu}} = \mathbf{0.1}$, $\boldsymbol{F_{0\mu}} = \mathbf{1}$, and $\boldsymbol{F_{1\mu}} = \mathbf{0.5}$ where **a**) shows $\boldsymbol{\Delta\theta(\tau)}$ and **b)** shows $\boldsymbol{\theta'(0,\tau)}$.

4. RESULTS

After several simulations, data is collected and plotted against non-dimensional time. The key parameters that are varied are the Biot number, Bi_{μ}, and the constants $F_{0\mu}$, and $F_{1\mu}$. This provides a broad scope of material and temperature conditions that may be expected in both subsonic and hypersonic heat exchange scenarios. The results section is broken into two pieces for comparison of the temperature change across the plate as well as the heat flux at the top surface of the plate. A normal distribution was used for Bi with $\sigma = \frac{0.1\,Bi_{\mu}}{3}$ ensuring a $\pm$ 10% 3-sigma variation.

4.1. Non-Dimensional Temperature Difference Across the Plate

Figures **3** through **7** specifically display the non-dimensional temperature changes across the plate as non-dimensional time progresses. As Biot number increases, the general behavior of the non-dimensional temperature differences follows a similar trend. However, the primary characteristics to note are that the steady state values increase as Biot number increases. This is a similar trend found in another research, and is explained by the following:

$$\Delta\theta(\tau = \infty) = \frac{Bi}{1 + Bi} \quad (17)$$

The steady-state $\Delta\theta$ value at $\tau = 1000$ is determined by the value of Bi_{μ}.

The transient portion of this simulation for all cases lasts until a non-dimensional time of $\tau = 1$. Beyond that point, there is a distribution of outputs, but it is much less than the uncertainty observed earlier in each simulation. Additionally, the distribution in the later portion of the simulation is approximately uniform.

As focus shifts to other aspects of the simulation, it is interesting to compare simulations as $F_{0\mu}$ and $F_{1\mu}$ change individually. Across the 45 total simulations accomplished for $\Delta\theta$, as $F_{1\mu}$ changes, the stochastic spread changes very little. This is observed by comparing the groupings of data in each individual subplot. Instead, the different $F_{1\mu}$ terms have a greater impact on the initial values of $\Delta\theta$, therefore affecting the transient path of the simulation. On the other hand, as $F_{0\mu}$ increases, the amount of uncertainty in the transient results also increases. This is most obvious when Biot numbers are small, such as $Bi = 0.01$ depicted in Figure **3**. In this case, the variation in $\Delta\theta$ increased from a range of about 0.1 for $F_{0\mu} = 0.5$ to a range of about 0.45 when $F_{0\mu} = 2$. This becomes less apparent as Biot number increases and the magnitude of the Biot number itself drives the non-dimensional temperature change across the plate.

4.2. Non-Dimensional Heat Flux at Upper Surface of the Plate

The non-dimensional heat flux provides a different perspective on the one-dimensional problem than what is presented when only looking at the non-dimensional temperature difference. The parameters used for the non-dimensional heat flux are the same as those used in the non-dimensional temperature differences across the plate. Figures **8** through **12** are laid out and organized in the same manner as seen above.

As discussed with the data found for $\Delta\theta$, the Biot number primarily has an effect on the final value of $\theta'(0)$, which can be represented as shown in Eq. 18:

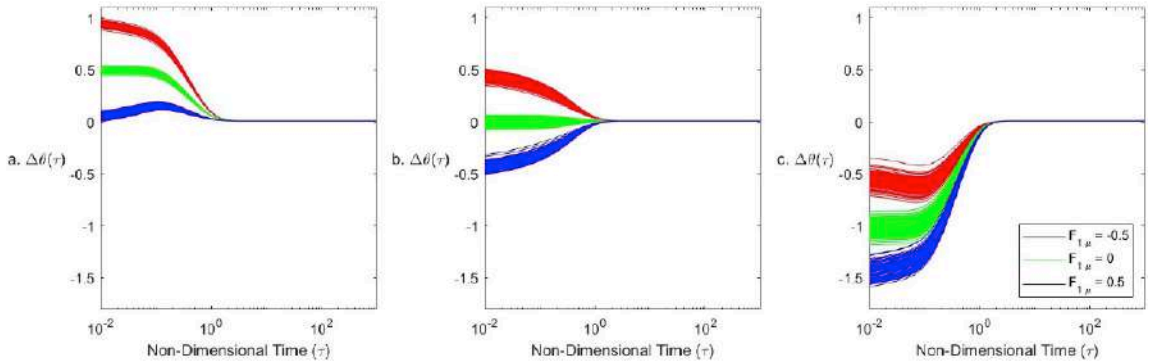

Figure 3: $\Delta\theta$ with $Bi_{\mu} = 0.01$ and a) $F_{0\mu} = 0.5$ b) $F_{0\mu} = 1$ c) $F_{0\mu} = 2$.

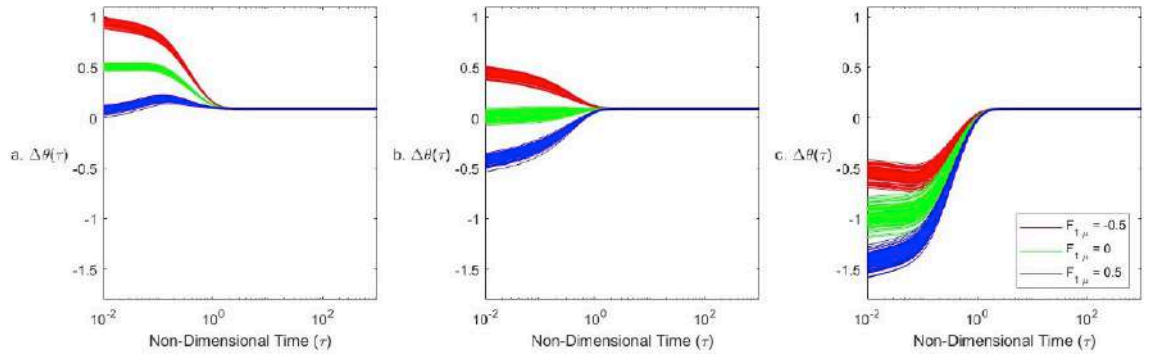

Figure 4: $\Delta\theta$ with $Bi_{\mu} = 0.1$ and a) $F_{0\mu} = 0.5$ b) $F_{0\mu} = 1$ c) $F_{0\mu} = 2$.

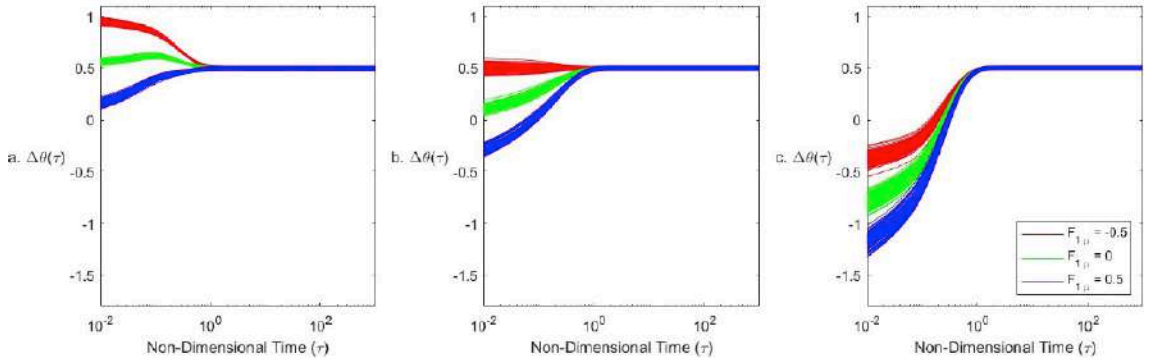

Figure 5: $\Delta\theta$ with $Bi_{\mu} = 1$ and a) $F_{0\mu} = 0.5$ b) $F_{0\mu} = 1$ c) $F_{0\mu} = 2$.

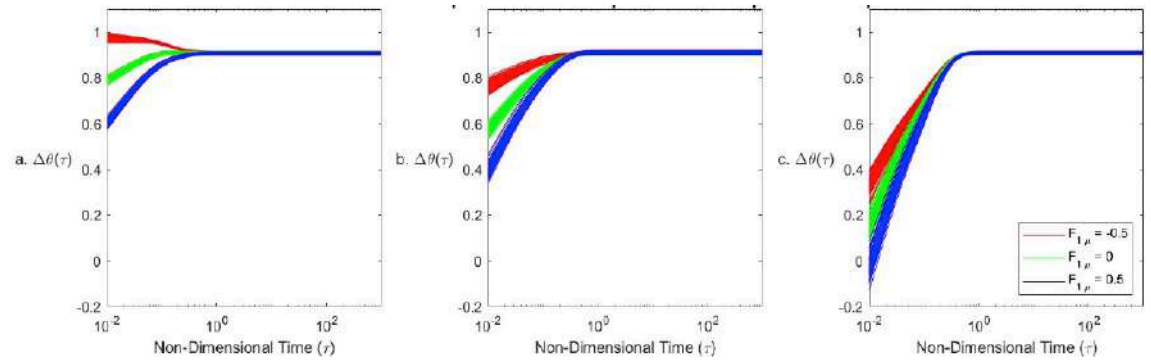

Figure 6: $\Delta\theta$ with $Bi_{\mu} = 10$ and a) $F_{0\mu} = 0.5$ b) $F_{0\mu} = 1$ c) $F_{0\mu} = 2$.

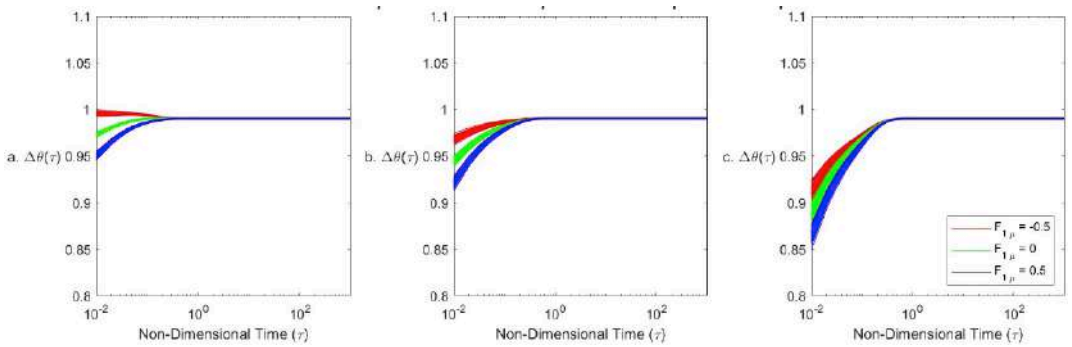

Figure 7: $\Delta\boldsymbol{\theta}$ with $\boldsymbol{Bi_\mu = 100}$ and a) $\boldsymbol{F_{0\mu} = 0.5}$ b) $\boldsymbol{F_{0\mu} = 1}$ c) $\boldsymbol{F_{0\mu} = 2}$.

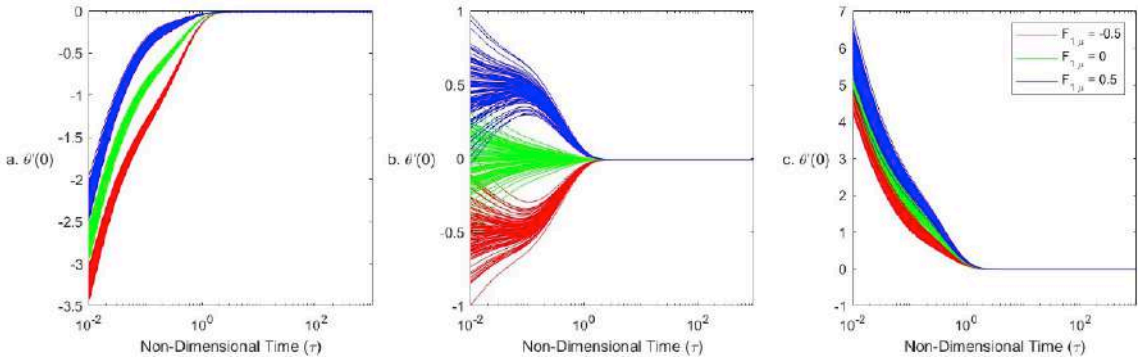

Figure 8: $\boldsymbol{\theta'(0,\tau)}$ with $\boldsymbol{Bi_\mu = 0.01}$ and a) $\boldsymbol{F_{0\mu} = 0.5}$ b) $\boldsymbol{F_{0\mu} = 1}$ c) $\boldsymbol{F_{0\mu} = 2}$.

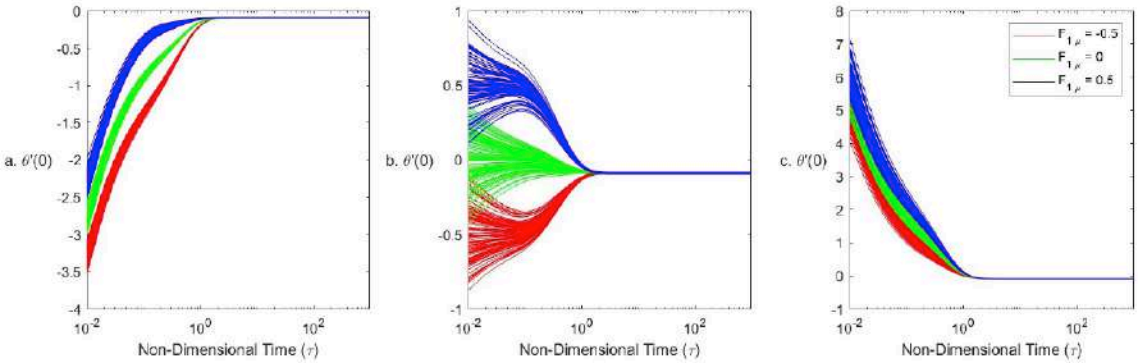

Figure 9: $\boldsymbol{\theta'(0,\tau)}$ with $\boldsymbol{Bi_\mu = 0.1}$ and a) $\boldsymbol{F_{0\mu} = 0.5}$ b) $\boldsymbol{F_{0\mu} = 1}$ c) $\boldsymbol{F_{0\mu} = 2}$.

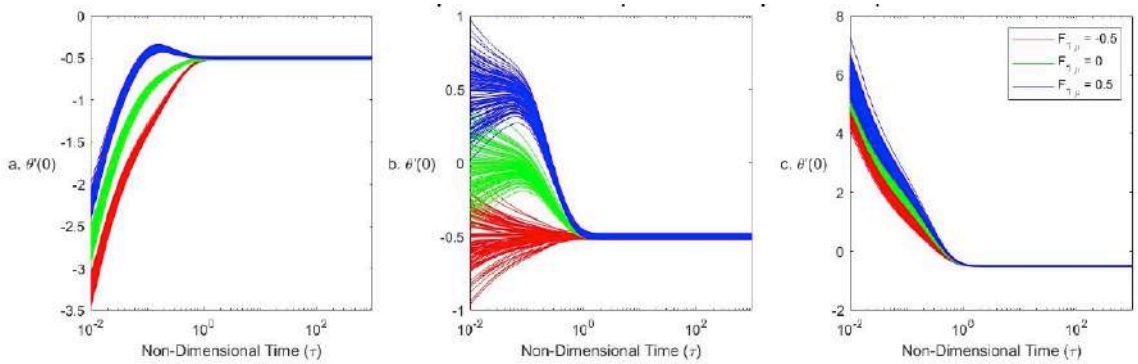

Figure 10: $\boldsymbol{\theta'(0,\tau)}$ with $\boldsymbol{Bi_\mu = 1}$ and **a)** $\boldsymbol{F_{0\mu} = 0.5}$ **b)** $\boldsymbol{F_{0\mu} = 1}$ **c)** $\boldsymbol{F_{0\mu} = 2}$.

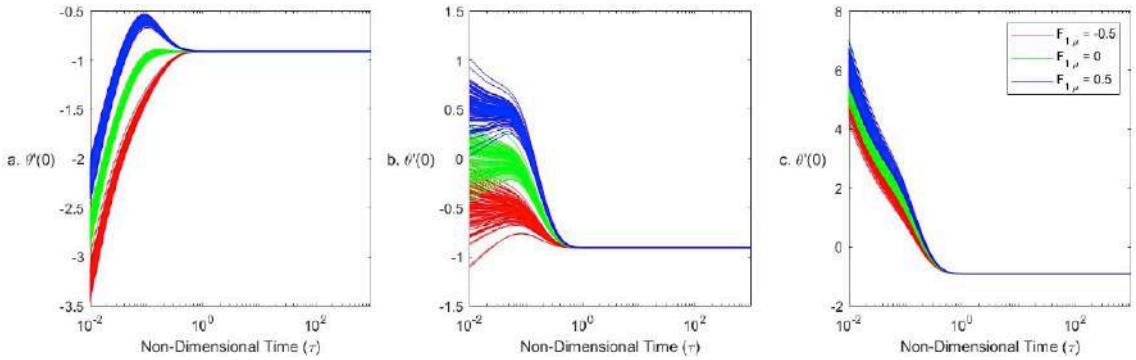

Figure 11: $\boldsymbol{\theta'(0,\tau)}$ with $\boldsymbol{Bi_\mu = 10}$ and a) $\boldsymbol{F_{0\mu} = 0.5}$ b) $\boldsymbol{F_{0\mu} = 1}$ c) $\boldsymbol{F_{0\mu} = 2}$.

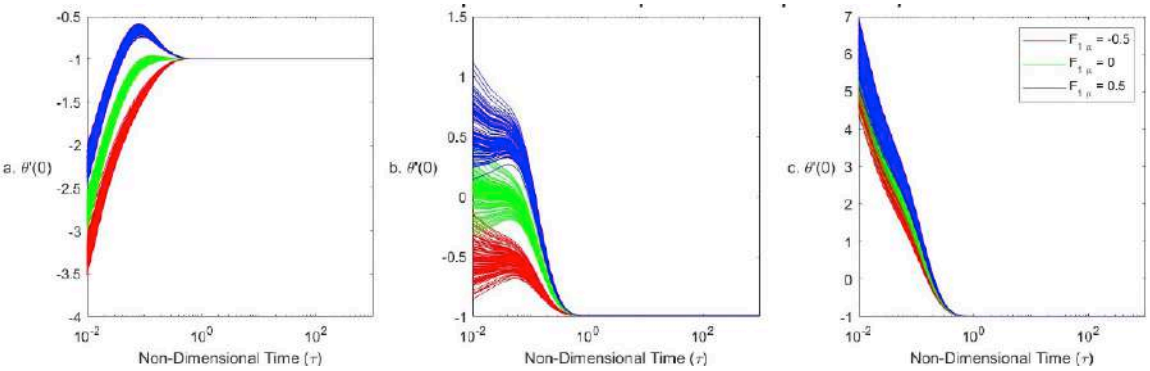

Figure 12: $\boldsymbol{\theta'(0,\tau)}$ with $\boldsymbol{Bi_\mu = 100}$ and a) $\boldsymbol{F_{0\mu} = 0.5}$ b) $\boldsymbol{F_{0\mu} = 1}$ c) $\boldsymbol{F_{0\mu} = 2}$.

$$\theta'(\tau = \infty) = -\frac{Bi}{1 + Bi} \quad (18)$$

However, in these simulations, the total uncertainty remains relatively consistent as Biot number changes. The value of $F_{1\mu}$ has little effect on the overall uncertainty of the transient response, but impacts the initial condition and path of the transients instead. At steady state, the initial conditions (F0, F1) decay and the solution is governed purely by the balance between internal conduction and external convection, which is captured by the Biot number.

When observing the effect of $F_{0\mu}$ on $\theta'(0)$, there is a much more noticeable change. With values of $F_{0\mu} = 0.5$, the uncertainty in $\theta'(0)$ is relatively low, and the general trend is an exponential decay with all negative values. With a value of $F_{0\mu} = 2$, the uncertainty in $\theta'(0)$ is also relatively low with an exponentially decaying trend. However in this case, all values for $\theta'(0)$ are positive. This suggests that the $F_{0\mu}$ term drives the direction of heat flux in these types of simulations.

For the third case, when $F_{0\mu} = 1$, the simulations provide much more variation in the outputs. In fact, the uncertainty in the initial state of $\theta'(0)$ is so great that the direction of heat flux may have different directions with all other conditions held the same. This quickly dampens out, and the final value reaches a constant when non-dimensional time $\tau = 1$. This uncertainty in the direction of heat flux may have further implications when applied to a real-life system. We note that $F_{0\mu} = 1$ implies that the initial temperature at the top surface is equal to the ambient temperature, making the heat flux at the boundary inherently ambiguous and highly sensitive to other stochastic inputs.

5. CONCLUSION

After several Monte-Carlo simulations for the one-dimensional plate setup, the behavior of the transient thermal management properties were documented and displayed. Uncertainty in the Biot number and the initial conditions of each simulation had an effect on the overall behavior of the interaction, but every simulation followed an exponentially decaying trend that ultimately reached a steady state value that had a small uniform distribution. Throughout each simulation, the uncertainty continuously decreased as time progressed.

The simulations that show the greatest variability in the $\Delta\theta$ are those with the highest values of $F_{0\mu}$, especially when the values of Biot numbers are low. The simulations that show the greatest variability in

$\theta'(0)$ are those where the value $F_{1\mu} = 1$. In most instances, the uncertainty in the Biot number and the initial conditions cause outputs that can be both positive and negative, leading to an unknown for the direction of heat flux in the system. This is one of the driving factors that may impact the designs of hypersonic vehicles and their associated cooling systems.

This research expands upon what has been explored in several other papers for uncertainty propagation in one dimensional heat transfer scenarios with different boundary conditions. Future research can go in several different directions. First, one-dimensional problems can continue to be explored with more boundary condition configurations, or with uncertainty in more variables in the problem. The boundary conditions more representative of aerodynamic heating can be considered. Next, two-dimensional heat transfer cases may be explored for more practical application to real life heat exchangers. Should others decide to quantify uncertainty propagation in two-dimensional problems, it may be necessary to look for ways to estimate the eigenvalues of the problem in the numerical method to increase computational efficiency by using sparse grid techniques. This would enable more complicated problems to be assessed and would also allow for a greater number of trials to be used in each simulation for greater accuracy.

NOMENCLATURE

A = constant

An = coefficients in non-dimensional time-dependent series

B = constant

Bi = Biot number, Lh / k

c_p = specific heat, $J / (kg \cdot K)$

F_0 = dimensionless constant parameterizing initial temperature

$F_{0\mu}$, $F_{1\mu}$ = mean values for stochastic quantities F_0, and F_1

F_1 = dimensionless constant parameterizing initial temperature distribution across plate

h = convective heat transfer coefficient, $W / (m^2 \cdot K)$

k = thermal conductivity, $W / (m \cdot K)$

L = thickness of plate, m

S = steady solution to problem

T = temperature, K

T^i = initial temperature on the top surface of the plate

T^∞ = temperature of ambient medium surrounding plate, K

t = time, s

U = unsteady solution to problem

x = dimensional coordinate, m

α = thermal diffusivity, m^2 / s

β_n = non-dimensional eigenvalue

$\Delta\theta$ = dimensionless temperature difference between the top and bottom surfaces of the plate

θ = dimensionless temperature

θ_{init} = initial dimensionless temperature

λ_n = dimensional eigenvalues

ξ = dimensionless coordinate, z / L

ρ = material density, kg / m^3

τ = dimensionless time, $\alpha t / L^2$

ACKNOWLEDGEMENTS

The authors would like to acknowledge the funded collaboration between the Aerospace Vehicles Division of the Aerospace Systems Directorate and the Air Force Institute of Technology, and the support of the Air Force Office of Scientific Research through a Lab Task monitored by Dr. Fariba Fahroo.

REFERENCES

[1] Bertin JJ, Cummings RM. Aerodynamics for Engineers, Cambridge University Press 2022.

[2] Ferretto D, Viola N. Preliminary Design and Simulation of a Thermal Management System with Integrated Secondary Power Generation Capability for a Mach 8 Aircraft Concept Exploiting Liquid Hydrogen. Aerospace 2023; 10. https://doi.org/10.3390/aerospace10020180

[3] Forster EE, Clark DL, Beran PS. Evaluation of Designed Distributions for Stochastic Collocation Methods. AIAA SciTech Forum and Exposition 2023; 2023: 15. https://doi.org/10.2514/6.2023-0742

[4] Clark DL, Aksland CT, Lupp CA, Forster EE. Optimization under Uncertainty Techniques for Time-Dependent Aircraft Systems with Controllers 2023. https://doi.org/10.2514/6.2023-1095

[5] Panasyuk GY, Yerkes KL. Input Uncertainty and Implication for Modeling Generic and High-Fidelity Transient Convection Problems. Journal of Thermophysics and Heat Transfer 2022; 36. https://doi.org/10.2514/1.T6444

[6] Panasyuk GY, Yerkes KL. Modeling of Uncertainty Propagation for Transient Heat Rejection Problems. Journal of Thermophysics and Heat Transfer 2024; 38. https://doi.org/10.2514/1.T6820

[7] Carslaw HS, Jaeger JC. Conduction of heat in solids Second Edition, Oxford Science Publications 1959.

Received on 25-06-2025 Accepted on 26-09-2025 Published on 27-10-2025

https://doi.org/10.66000/3110-9780.2025.01.02

© 2025 Muff *et al*.
This is an open access article licensed under the terms of the Creative Commons Attribution License (http://creativecommons.org/licenses/by/4.0/) which permits unrestricted use, distribution and reproduction in any medium, provided the work is properly cited.